Influence of stress on Raman spectra in $Ba_{1-x}Sr_xTiO_3$ thin films

2006 J. Phys. D: Appl. Phys. 39 2819

(http://iopscience.iop.org/0022-3727/39/13/027)

INSTITUTE OF PHYSICS PUBLISHING JOURNAL OF PHYSICS D: APPLIED PHYSICS

J. Phys. D: Appl. Phys. **39** (2006) 2819–2823 doi:10.1088/0022-3727/39/13/027

Influence of stress on Raman spectra in $Ba_{1-x}Sr_xTiO_3$ thin films

L Z Cao[1], B L Cheng[1], S Y Wang[1], W Y Fu[1], S Ding[1], Z H Sun[1], H T Yuan[2], Y L Zhou[1,3], Z H Chen[1] and G Z Yang[1]

[1] Beijing National Laboratory for Condensed Matter Physics, Institute of Physics, Chinese Academy of Sciences, Beijing 100080, People's Republic of China

[2] Changchun Institute of Optics, Fine Mechanics and Physics, Chinese Academy of Sciences, Changchun 130033, People's Republic of China

E-mail: ylzhou@aphy.iphy.ac.cn

Received 1 April 2006, in final form 3 April 2006
Published 16 June 2006
Online at stacks.iop.org/JPhysD/39/2819

Abstract

$Ba_{1-x}Sr_xTiO_3$ ($x = 0.3, 0.5, 0.7$) thin films have been prepared on (001) MgO substrates by pulsed laser deposition. Temperature-dependent permittivity and Raman spectra of the $Ba_{1-x}Sr_xTiO_3$ films are compared with those of the corresponding bulk samples. Raman spectra indicate that a tetragonal structure is present in the $Ba_{0.5}Sr_{0.5}TiO_3$ thin film while the $Ba_{0.5}Sr_{0.5}TiO_3$ bulk sample shows a cubic structure. Temperature-dependent permittivity shows that the phase transition in the film occurs over a wide temperature range, which results in the co-existence of the cubic phase and tetragonal phase in the $Ba_{0.5}Sr_{0.5}TiO_3$ film. The smooth change of phase transition is attributed to the residual stress in the film. We demonstrate that the residual stress releases gradually with increasing thickness of the film. Furthermore, the effects of the composition and thickness on Raman spectra have also been discussed systematically.

1. Introduction

Recently, $Ba_{1-x}Sr_xTiO_3$ (BST-x) thin films have received considerable attention for applications such as high-density dynamic random access memories (DRAMs), phase shifters and room-temperature pyroelectric infrared detectors [1–4]. In such devices, the dielectric and optical properties of the films are significantly influenced by the internal stress [5]. Raman spectra have been demonstrated as a powerful tool to study internal stress, which causes variation in phonon frequencies and life times, leading to broadening of Raman peaks and breakdown of the Raman selection rule. Now, much effort has been focused on Raman spectra of the BST films. There have been many reports on the temperature-dependent and composition-dependent Raman spectra of BST-x materials [6–11]. Tenne *et al* reported the Raman spectra of the BST-x thin films with $x = 0.05, 0.1, 0.2, 0.35$ and 0.5 in the temperature range from 5 to 300 K [8]. They observed the differences in the lattice-dynamical properties between thin films and the corresponding single crystals and concluded that the presence of the polar nanoregions in the films at the temperature above the bulk ferroelectric phase transition resulted in the specific lattice-dynamical properties of the BST films.

In our recent work, we have successfully applied Raman spectra to investigate the internal stress in $BaTiO_3$ and BST films. Guo *et al* studied the Raman peaks of $BaTiO_{3-x}$ thin films deposited under different oxygen pressure from 10^{-2} to 10^{-5} Pa [12]. Raman peaks at 532 and 742 cm^{-1} shifted towards the lower frequency with decreasing oxygen pressure, suggesting a decrease in internal stress in $BaTiO_{3-x}$ thin films. At the same time, the main Raman peaks became broadened, which might be attributed to structural disorder in the $BaTiO_{3-x}$ lattice structure. Wang *et al* reported Raman spectra of multilayered compositional graded $(Ba_{0.8}Sr_{0.2})$ $(Ti_{1-x}$ $Zr_x)O_3$ (BSTZ) thin films [13]. They observed that the Raman peaks at 535 and 750 cm^{-1} shifted to high frequency with increasing compositional gradient, which might be attributed to the increasing internal stress in the multilayered BSTZ thin film. Wang *et al* reported that the peaks at 226, 524 and 733 cm^{-1} shifted to high frequency in the Raman spectra of Ce-doped BST films, which

[3] Author to whom any correspondence should be addressed.

indicated the variation of internal stress in the film [14]. In addition to oxygen pressure, doping and the multilayered structure, there are many other factors which influence stress in the BST films, such as composition, thickness, etc. In this paper, we report the composition-dependent and thickness-dependent Raman spectra of BST films. Effects of stress in the films are systematically investigated. Moreover, temperature-dependent permittivity is measured in order to understand the presence of the tetragonal phase in the BST-0.5 film.

2. Experimental

A conventional ceramic processing was used to prepare the BST target for pulsed laser deposition (PLD); and the detailed information has been described elsewhere [11, 15]. The PLD experiment was performed using a XeCl excimer laser system with an average pulse energy of 200 mJ. The deposition of $Ba_{1-x}Sr_xTiO_3$ film was carried out at a substrate temperature of 800° with an oxygen pressure of 30 Pa, and the samples were subsequently annealed at 600° for 20 min.

The thickness of the films was measured by a surface profiler of Dektak-8. The crystal structure of the thin films was determined by x-ray diffraction (XRD), using Cu$K\alpha$ radiation with a wavelength of 1.5405 nm. Raman measurements for the samples were performed at room temperature in the back scattering geometry with a Jobin–Yvon T64000 triple Raman spectrometer. A 488 nm Ar^+ ion laser line of 100 mW was used for the excitation. The incident light and the scattering light were perpendicular to the surface of the sample. The spectrometer provided a wave number resolution of $\sim$0.5 cm^{-1} and accuracy of $\sim$1 cm^{-1}. Temperature-dependent permittivity of the BST film was measured by an Agilent 4294A precision impedance analyser, using the conventional interdigital electrode (IDE) method.

3. Results and discussion

3.1. Bulk samples

XRD profiles of BST-x ($x = 0.3, 0.5, 0.7$) bulk samples are measured (not shown here). The XRD patterns indicate that BST-0.3 has a tetragonal structure while the other two samples have a cubic structure, which is also demonstrated by the temperature-dependent permittivity result.

The permittivity of the BST-x ($x = 0.3, 0.5, 0.7$) ceramics as a function of temperature is shown in figure 1. As an example, for the BST-0.5 bulk sample, there are phase transition peaks P_1, P_2, P_3 located at about 154, 192 and 244 K corresponding to the phase transitions from the rhombohedral to orthorhombic, orthorhombic to tetragonal, tetragonal to cubic, respectively [16]. Similar behaviours can be found in BST-0.3 and BST-0.7 samples in figure 1. The Curie temperature, T_c, decreases from 314 K to 244 K and to 179 K for the BST-0.3, BST-0.5 and BST-0.7 bulk samples, respectively. The results show that the bulk sample of BST-0.3 is in the tetragonal phase, while BST-0.5 and BST-0.7 are in the cubic phase at room temperature. In order to compare with the film samples, it is necessary to note that the phase transitions in the bulk samples are very clear and sharp.

Raman spectra of BST-x ($x = 0.3, 0.5, 0.7$) bulks at room temperature are shown in figure 2. Phonon frequencies (ω)

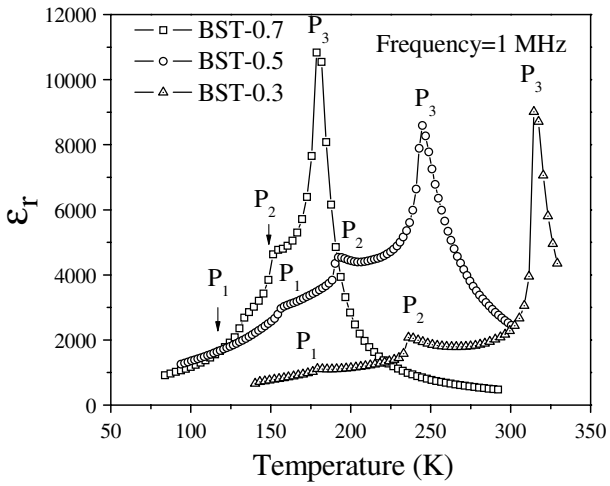

Figure 1. Permittivity of BST-0.3, BST-0.5 and BST-0.7 bulk samples as a function of temperature.

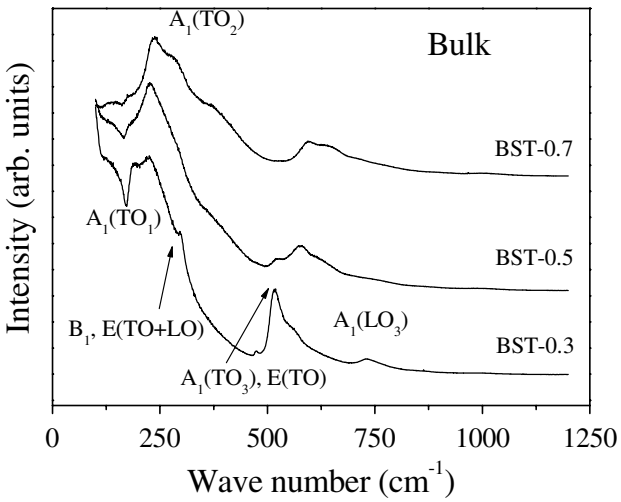

Figure 2. Room temperature Raman spectra of BST-0.3, BST-0.5 and BST-0.7 bulk samples.

and their mode assignments in the BST-0.3 bulk sample are summarized in table 1. First, in the Raman spectra of BST-0.3, a strong peak at 221 cm^{-1} assigned to $A_1(TO_2)$ mode, and an asymmetric band near 516 cm^{-1} in which both $A_1(TO_3)$ and E(TO) modes seem to be present are observed. With the increasing Sr concentration, the Raman peaks become broad and gradually lose their intensity. In the Raman spectra of BST-0.7, the peak at 516 cm^{-1} is seen to disappear completely and a broad peak at 548 cm^{-1} is observed. It is known that Raman peaks should not be present in the ideal cubic phase, and whether the origin of these bands in the cubic phase is from disorder-induced, first-order or second-order Raman scattering has been discussed. A recent temperature-dependent Raman study on single crystalline $BaTiO_3$ has shown that these broad bands in the cubic phase are first-order in character [7]. The broadened spectra observed in the Raman spectra of BST-0.7 indicates that the Raman selection rule is relaxed, which we ascribed to the disorder in the positions of the Ti atoms in the unit cells of the polycrystalline samples [17]. Second, in Raman spectra of the BST-0.3 film, we observe a shoulder at 294 cm^{-1}, which might be attributed to the B_1 and E(TO_2)

Table 1. Phonon frequencies (ω) and their mode assignment in the BST-0.3 bulk sample.

ω (cm^{-1})	176	221	294	516	732
Mode	$A_1(TO_1)$	$A_1(TO_2)$	B_1, E(TO+LO)	$A_1(TO_3)$, E(TO)	ss$A_1(LO_3)$

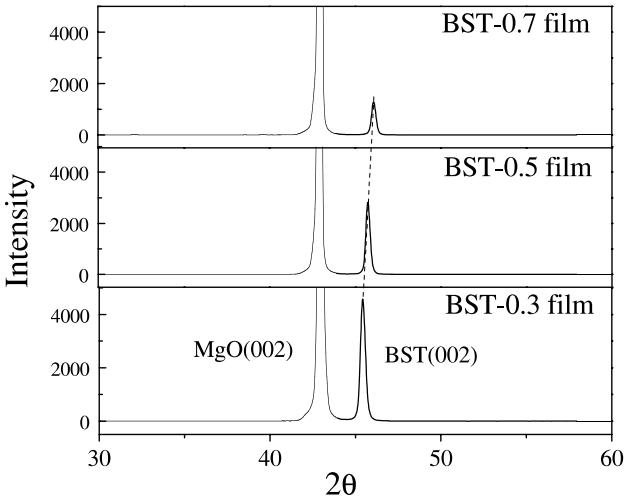

Figure 3. XRD patterns of $Ba_{1-x}Sr_xTiO_3$ ($x = 0.3, 0.5, 0.7$) films on the MgO substrate.

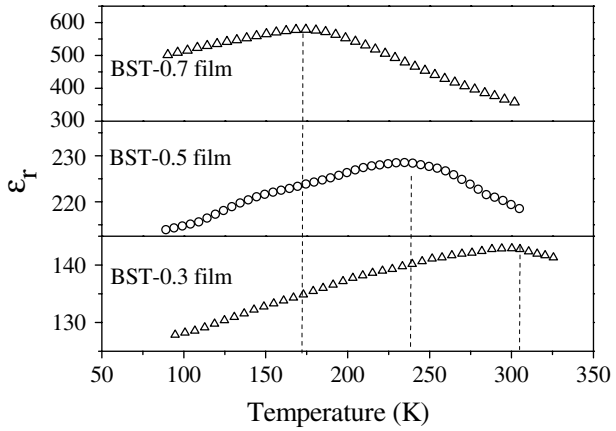

Figure 4. Permittivity of BST-0.3, BST-0.5 and BST-0.7 thin films as a function of temperature.

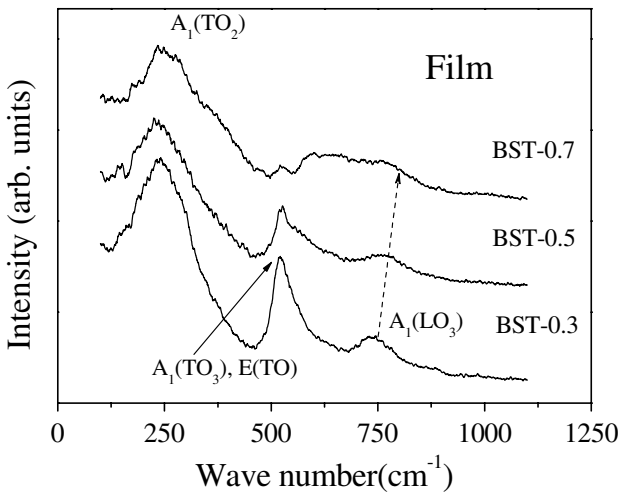

Figure 5. Room temperature Raman spectra of BST-0.3, BST-0.5 and BST-0.7 thin films.

modes and the highest frequency peak near 732 cm^{-1} in which the $A_1(LO_3)$ mode seems to be present. It is known that this peak is specific to the tetragonal phase of the BST material [7]. Then, we draw the same conclusion with the result of the XRD and temperature-dependent permittivity.

3.2. Film samples

XRD profiles of the BST-x ($x = 0.3, 0.5, 0.7$) films are shown in figure 3. The films have preferred orientation along the (001) direction due to the (001) MgO substrate. With the increasing Sr concentration, the diffraction peaks (00k) of the BST films shift to high angle and the intensity of the (002) peaks decrease gradually. The lattice parameters (c) along the vertical-substrate direction are 3.988, 3.952 and 3.934 Å for the BST-0.3, BST-0.5 and BST-0.7 films, respectively. It is known that MgO has a cubic structure with $a = 4.213$ Å. The decrease in the intensity of the (00k) peaks may be attributed to the increasing lattice mismatch between the MgO substrate and the BST-x film.

From the XRD patterns, we cannot obtain detailed information about the structure of the samples. Then temperature-dependent permittivity of the films is measured, as shown in figure 4. Compared with those of the bulk samples, the peaks of permittivity are significantly broadened, and other phase transitions are hardly discernible except for the ferroelectric transition in the films. Such broad peaks are typical for diffuse transitions as observed in some epitaxial BST thin films. There are many hypotheses proposed to explain the observed smearing of the phase transition [18]. Recently, Bratkovsky and Levanyuk described a new mechanism of strong phase transition smearing in thin films where the surface acts as a defect coupled to the order parameter [19]. Parker *et al* also observed the diffuseness of the dielectric anomaly and believed that the broadened dielectric anomaly indicated that the phase transition occurred over a wide temperature range [20]. As shown in figure 4, the main phase in the BST-0.3 film is tetragonal, and other two samples are cubic in room temperature. But because the phase transition occurs over a wide temperature range, other phases may be present in the film besides the main phase.

Room-temperature Raman spectra of BST-x ($x = 0.3, 0.5, 0.7$) films with a thickness of around 300 nm are plotted in figure 5. Optical phonons of the MgO bulk are Raman inactive due to crystal symmetry, so the substrate should have no effect on the Raman signals of the thin film. First, the weak peak related to the $A_1(TO_3)$ and E(TO) modes is still observed in Raman spectra of the BST-0.7 film, while the peak completely disappears in the BST-0.7 bulk sample. Moreover, the peak observed at about 548 cm^{-1} in the bulk samples is very weak in BST-0.7 film samples, which only shows a distinguishable shoulder. Second, the peak related to the $A_1(LO_3)$ mode is present in Raman spectra of the

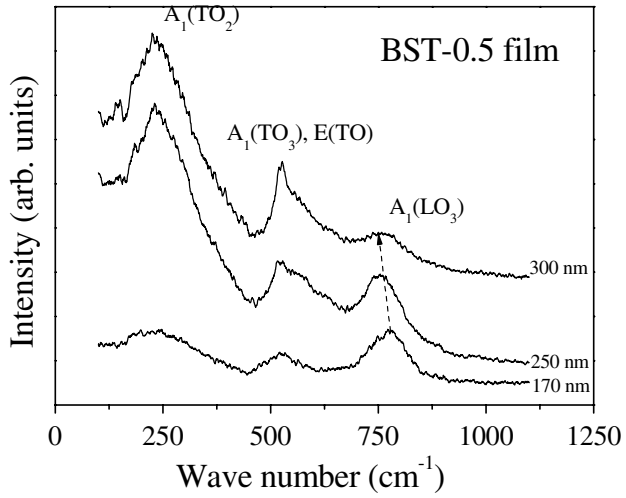

Figure 6. Thickness-dependent Raman spectra of BST-0.5 thin films.

BST-0.3 film. We observe that the peak is located at a higher wave number (739 cm^{-1}) than the corresponding bulk samples (732 cm^{-1}) which can be attributed to the tensile stress in the film [21]. Furthermore, the peak is still present in the Raman spectra of the BST-0.5 film, and it shifts to higher frequency compared with the BST-0.3 film. It is known that the phonon frequencies are composition dependent with respect to BST films [8, 17]. Moreover; the tensile stress in the films might be responsible for the shift towards high wave number of the Raman peaks partially, which will be discussed in detail below.

The peak related to the $A_1(LO_3)$ modes confirms the presence of a tetragonal structure in the BST-0.5 film. The result of temperature-dependent permittivity of the films also indicates that the phase transition in the film occurs over a wide temperature range. We propose that such a smooth change of phase transition results in the coexistence of the cubic phase and tetragonal phase in our BST-0.5 film. The main phase in the BST-0.5 film is cubic, and the tetragonal phase is presented in a certain region, which is similar to the polar nano-regions in the film.

Figure 6 shows the Raman spectra of BST-0.5 thin films of different thicknesses (170, 250 and 300 nm) deposited under the same condition. With increasing thickness, the peak at 730 cm^{-1} loses its intensity gradually, while other peaks increase their intensities. Moreover, the peak related to the $A_1(LO_3)$ shifts to low frequency. Zhu *et al* observed a similar phenomenon, and they attributed it to the effect of tensile stress [21]. In our samples, with increasing thickness, the stress in the BST-0.5 film is released gradually, which might account for the variation of intensity and the shift towards low wave number of Raman peaks. As circumstantial evidence, we simply calculate the lattice constant according to the position of the (002) peak of BST films in the XRD patterns. The lattice parameters (c) are 3.968 Å, 3.954 Å and 3.952 Å for the 170 nm, 250 nm and 300 nm films, respectively. We know that the lattice constant of the BST-0.5 bulk is 3.952 Å. The gradually approached lattice constant indicates that the stress in the film is released with increasing thickness.

According to the elastic compliance tensor, we can separate residual stress into biaxial stress and hydrostatic stress, i.e. the stress caused by the lattice mismatch or thermal mismatch and the stress originating from oxygen vacancies or doping, respectively. The hydrostatic stress can affect all three axes of the unit cell, while the biaxial stress affects the two in-plane axes directly and out-of-plane axes through the Poisson ratio. For the BST thin films on MgO, the lattice of film may be expanded near the interface to match the large lattice of the substrate and consequently tensile stress may remain in the BST film. In the process of cooling from the deposition temperature, BST films are compressive due to thermal coefficient mismatch on cooling. Furthermore, the variation of compositions and oxygen vacancies also result in variation of the lattice, which may induce stress in the BST film. Therefore, there are three competing forces affecting the stress state in the film. The stress induced by the lattice mismatch ($x_l = (a_s - a_f)/a_f$) and thermal expansion mismatch ($x_t = (a_s' - a_f') \times \Delta T$) are considered to play major part in stress formation. In the stress expression of x_l and x_t, a_s (4.213 Å) and a_f (3.952 Å) are the equilibrium lattice, while $a_s'(13.8 \times 10^{-6}/^{\circ}C)$ and $a_f'(10.5 \times 10^{-6}/^{\circ}C)$ are the thermal expansion coefficients of the substrate and BST films [14]. Because of the same deposition parameters in our experiment, the stress caused by the oxygen vacancies and thermal expansion mismatch might be the same. As discussed above, the lattice of the BST thin films is compressed with increasing Sr concentration. Thus, the tensile stress deduced from the lattice compression might be responsible for the shift towards a high wave number of the Raman peak as shown in figure 5. And the Raman peak related to $A_1(LO_3)$ mode shifts to lower frequency with increasing thickness of the films as shown in figure 6, which we attribute to the release of tensile stress in the films.

Besides this work, such stress analysis works well with many other BST/MgO systems. As observed in films deposited under different oxygen pressures, the lattice of $BaTiO_{3-x}$ expanded with the increasing density of oxygen vacancies resulting from decreasing oxygen pressure [12]. The expanded lattice was followed by the release of residual stress, which resulted in the shift towards a low wave number of the Raman peaks related to the $A_1(LO_3)$ mode. In the case of a multilayered structure, it was reasonable to propose that the more compositional gradient the films contained, the more difficult the release of the tensile stress. Consequently, the Raman peak of the $A_1(LO_3)$ mode shifted to higher frequency with increasing composition gradient [13].

4. Conclusions

In summary, we have investigated the Raman spectra of BST-x ($x = 0.3, 0.5, 0.7$) films prepared by pulsed laser deposition on MgO substrates. The analysis of the Raman spectra under various mole fractions of Sr indicates that there is a delay of the phase transition in films compared with the corresponding bulk samples, which might be attributed to the residual stress in the films. Temperature-dependent permittivity of the films and bulk samples show that the phase transition in the film is a smooth change, which results in the coexistence of the cubic phase and tetragonal phase in our BST-0.5 film. We find that the residual stress releases gradually with the increasing thickness. Furthermore, the effects of composition

and thickness on Raman spectra have also been discussed systematically.

Acknowledgments

This work is supported by the National Natural Science Foundation of China (60371032). The authors would like to thank M Lei and X H Zhu for their stimulating discussions.

References

[1] Jin F, Auner G W, Naik R, Schubring N W, Mantese J V, Catalan A B and Micheli A L 1998 *Appl. Phys. Lett.* **73** 2838
[2] Chang W T, Gilmore C M, Kim W J, Pond J M, Kirchoefer S W, Qadri S B, Chirsey D B and Horwitz J S 2000 *J. Appl. Phys.* **87** 3044
[3] Kingon A I, Streiffer S K, Basceri C and Summerfelt S R 1996 *Mater. Res. Bull.* **21** 46
[4] Streiffer S K, Basceri C, Parker C B, Lash S E and Kingon A I 1999 *J. Appl. Phys.* **86** 4565
[5] Chen M S, Shen Z X, Tang S H, Shi W S, Cui D F and Chen Z H 2000 *J. Phys.: Condens. Matter* **12** 7013
[6] Dobal P S, Dixit A, Katiyar R S, Garcia D, Guo R and Bhalla A S 2001 *J. Raman Spectrosc.* **32** 147
[7] Naik R *et al* 2000 *Phys. Rev.* B **61** 11367
[8] Tenne D A, Soukiassian A, Xi X X, Choosuwan H, Guo R and Bhalla A S 2004 *J. Appl. Phys.* **96** 6597
[9] Tenne D A, Clark A M, James A R, Chen K and Xi X X 2001 *Appl. Phys. Lett.* **79** 3836
[10] Yuzyuk Y I, Alyoshin V A, Zakharchenko I N, Sviridov E V, Almeida A and Chaves M R 2002 *Phys. Rev.* B **65** 134107
[11] Wang S Y, Cheng B L, Wang C, Peng W, Dai S Y and Chen Z H 2005 *Key Eng. Mater.* **280–283** 81
[12] Guo H Z, Chen Z H, Cheng B L, Lu H B, Liu L F and Zhou Y 2005 *J. Eur. Ceram. Soc.* **25** 2347
[13] Wang C, Cheng B L, Wang S Y, Dai S Y and Chen Z H 2005 *Key Eng. Mater.* **280–283** 1909
[14] Wang S Y, Cheng B L, Wang C, Dai S Y, Jin K J, Zhou Y L, Lu H B, Chen Z H and Yang G Z 2006 *J. Appl. Phys.* **99** 013504
[15] Cao L Z, Cheng B L, Wang S Y, Zhou Y L, Jin K J, Lu H B, Chen Z H and Yang G Z 2005 *J. Appl. Phys.* **98** 034106
[16] Cheng B L, Su B, Holmes J E, Button T W, Gabbay M and Fantozzi G 2002 *J. Electroceram.* **9** 17
[17] Kuo S Y, Liao W Y and Hsieh W F 2001 *Phys. Rev.* B **64** 224103
[18] Lookman A, Bowman R M, Gregg J M, Kut J, Rios S, Dawber M, Ruediger A and Scott J F 2004 *J. Appl. Phys.* **96** 555
[19] Bratkovsky A M and Levanyuk A P 2005 *Phys. Rev. Lett.* **94** 107601
[20] Parker C B, Maria J P and Kingon A I 2002 *Appl. Phys. Lett.* **81** 340
[21] Zhu J S, Lu X M, Jiang W, Tian W, Zhu M, Zhang M S, Chen X B, Liu X and Wang Y N 1997 *J. Appl. Phys.* **81** 1392